Biodistribution of Amino-Functionalized Diamond Nanoparticles. *In Vivo* Studies Based on ^{18}F Radionuclide Emission

Santiago Rojas,[†,#] Juan D. Gispert,[†,‡,#] Roberto Martín,[§] Sergio Abad,[⊥] Cristina Menchón,[⊥] Deborah Pareto,[†,‡] Víctor M. Víctor,[∥,△] Mercedes Álvaro,[§] Hermenegildo García,[§,*] and J. Raúl Herance[†,*]

[†]Institut d'Alta Tecnologia—Parc de Recerca Biomèdica de Barcelona, CRC Corporació Sanitària, 08003 Barcelona, Spain, [‡]Centro de Investigación Biomédica en Red en Bioingeniería, Biomateriales y Nanomedicina (CIBER BBN), 50018, Zaragoza, Spain, [§]Instituto Universitario de Tecnología Química CSIC-UPV, Universidad Politécnica de Valencia, Avenida de los Naranjos s/n, 46022 Valencia, Spain, [⊥]CRC Centre d'Imatge Molecular, CRC Corporació Sanitària, 08003 Barcelona, Spain, [∥]University Hospital Doctor Peset Foundation and CIBERehd, 46017, Valencia, Spain, and [△]Department of Physiology, University of Valencia, 46010, Valencia, Spain. [#]These authors have equally contributed to this work.

ABSTRACT Nanoparticles have been proposed for several biomedical applications; however, *in vivo* biodistribution studies to confirm their potential are scarce. Nanodiamonds are carbon nanoparticles that have been recently proposed as a promising biomaterial. In this study, we labeled nanodiamonds with ^{18}F to study their *in vivo* biodistribution by positron emission tomography. Moreover, the impact on the biodistribution of their kinetic particle size and of the surfactant agents has been evaluated. Radiolabeled diamond nanoparticles accumulated mainly in the lung, spleen, and liver and were excreted into the urinary tract. The addition of surfactant agents did not lead to significant changes in this pattern, with the exception of a slight reduction in the urinary excretion rate. On the other hand, after filtration of the radiolabeled diamond nanoparticles to remove those with a larger kinetic size, the uptake in the lung and spleen was completely inhibited and significantly reduced in the liver.

KEYWORDS: nanodiamonds · PET · pharmacokinetics · *in vivo* evaluation · rodent · surfactant · filtration

The development of novel materials for biological and biomedical applications has attracted a great amount of attention during the last years. For example, ferrous nanoparticles are used as contrast agents in magnetic resonance imaging, and different nanomaterials are under investigation to act as drug delivery systems in oncology in order to reduce the toxicity of chemotherapeutics.[1] The general requirements for these materials include good biocompatibility, sufficient blood residence time to reach the target, fast clearance from the body, and high accumulation in the target organs to be therapeutically efficacious with minimum side effects.[2] Among the multiple applications proposed for such materials,[3] probably the one receiving the most attention nowadays is their use as drug delivery systems to control the release of an active therapeutic drug into a specific target.[4] In particular, nanomaterials have been proposed to selectively release chemotherapics into tumors while the exposure to the rest of the organs is kept at a minimum. Most of the studies describing the use of nanomaterials as drug delivery systems have been carried out *in vitro* using cell cultures to test their toxicity and internalization,[5] while, to determine their actual potential in biomedical applications, *in vivo* biodistribution studies are mandatory. In this regard, several parameters influence the fate of nanomaterials in a living body such as particle size, composition, surface coating, solubility, and the presence or absence of a directing agent attached to their structure.[6]

Some techniques such as *post mortem* nanoparticle determination and *in vivo* optical imaging have been used to evaluate the biodistribution of nanocompounds.[7,8] Nevertheless, isotopic labeling with radioactive elements has been shown to be superior to evaluate pharmacokinetics and biodistribution in preclinical and clinical research,[9] as they are extremely sensitive and enable absolute quantification of the compound. The labeled compound can be injected into living animals, which are subsequently sacrificed at different time points to collect the organs and quantify their radioactivity content.[10] Alternatively, studies can be performed *in vivo* with single photon emission computed tomography (SPECT)[11] or positron emission tomography (PET)[12] in both laboratory animals and

* Address correspondence to rherance@crccorp.es.

Received for review March 15, 2011 and accepted June 9, 2011.

Published online June 09, 2011
10.1021/nn200986z

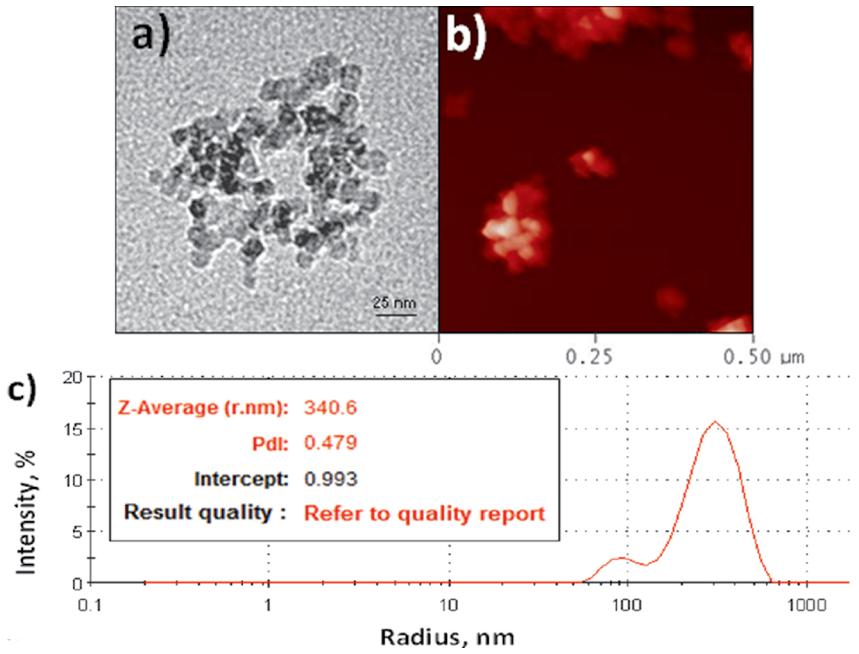

Figure 1. (a) TEM representative picture showing an aggregate of NH_2-npD. (b) The size of these aggregates was also confirmed by AFM. (c) LASER scattering experiment showing the particle size distribution of an aqueous suspension of NH_2-npD.

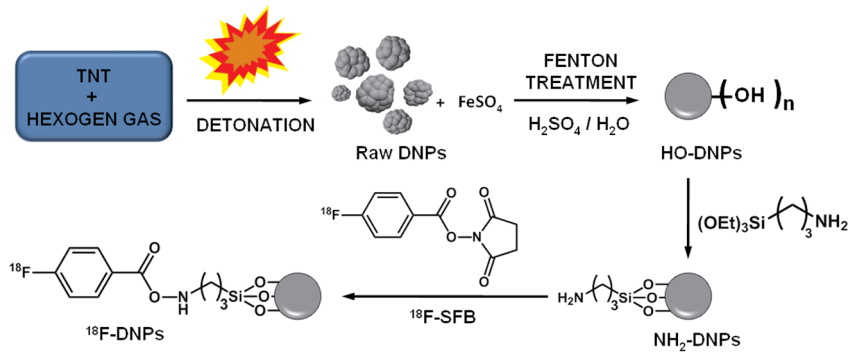

Figure 2. Scheme of nanodiamond production.

humans. However the *in vivo* imaging methods provide a limited spatial resolution that could be a limitation for the quantification of small tissues or organs in small animals.

Nanodiamonds (DNPs) are sp^3-carbon nanoparticles that have been recently proposed as a promising biomaterial since they present good biocompatibility, ability to cross the cell membrane, and capability to be functionalized to act as carriers.[13] These carbon nanocomposites are commercially available, as they can be obtained in large quantities by explosive detonation.[14] In order to increase their solubility in aqueous media and reduce particle aggregation, commercial DNPs are submitted to a Fenton treatment with hydrogen peroxide in order to remove the soot matrix that embeds DNP, forming large aggregates.[5] In addition, the Fenton reaction also produces hydroxyl radicals, which reduce the initial particle size from the 20 nm of the commercial sample to about 7 nm on average. Additionally, the surface of the treated DNPs has a large population of hydroxyl groups, and, thus, they will be denoted from now on as HO-DNPs.

In this work we present the first rodent biodistribution study of Fenton-treated HO-DNPs that have been functionalized with amino groups and in which syntons containing radioactive ^{18}F atoms have been anchored. Herein we study the influence of the nanomaterial size and formulation in the biodistribution of such compounds.

RESULTS AND DISCUSSION

Preparation of Radioactive ^{18}F-Labeled DNPs. The potential application of DNPs in several biomedical fields has been previously described.[16−18] However, to confirm their true potential in biomedical applications, *in vivo* biodistribution studies of nanoparticles are mandatory. In addition, the influence of formulation parameters such as the size and presence of surfactants needs to

be assessed and optimized. Previously, purification by the Fenton reaction has been reported to remove the amorphous soot matter and to form hydroxyl groups on the nanoparticle surface. Consequently, a reduction of the average particle size is achieved by chemical surface erosion.[18] The presence of surface OH groups in the Fenton-treated DNPs allows covalent anchoring of different molecules by conventional organic reactions. Previous studies have shown the feasibility of attaching long-chain alkyl groups by esterification of the surface OH groups or anchoring of aromatic compounds by a modification of the classical Friedel–Crafts reaction.[5]

In the present study, we have covalently attached ω-aminopropyl groups to the surface of HO-DNPs by means of the reaction of ω-aminopropyl trietoxysilane with the surface OH groups. This reaction occurs with high yields under mild conditions.[17] Silylation of surface OH groups is a well-established methodology in surface chemistry to functionalize different solid materials including silicas and metal oxides. The resulting amino-DNPs were treated with ^{18}F-SFB, thus achieving ^{18}F-radiolabeled nanoparticles to asses their biodistribution in living rodents.

Nanoparticles tend to spontaneously aggregate in aqueous solutions due to hydrophobic/hydrophilic forces experienced in water. Therefore, it has to be taken into consideration the difference between the

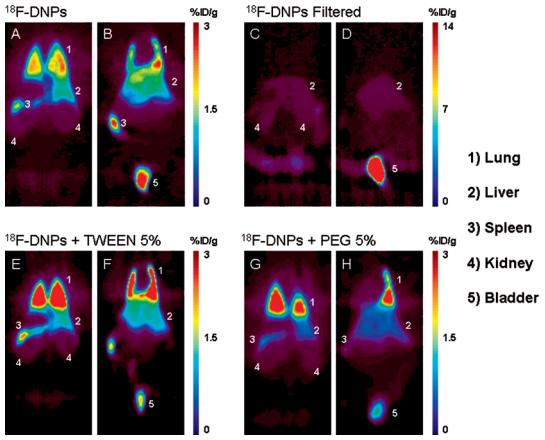

Figure 3. Coronal sections of PET images acquired 120 min after injection of the four different DNP preparations. Images show animals injected with ^{18}F-DNPs dorsal (A) to ventral (B), with filtered ^{18}F-DNPs dorsal (C) to ventral (D), with ^{18}F-DNPs + Tween 80 dorsal (E) to ventral (F), and finally with ^{18}F-DNPs + PEG$_{8000}$ dorsal (G) to ventral (H). Organs that presented elevated uptake of the radiolabeled compound are labeled with numbers for easy identification. Note the similar biodistribution pattern between ^{18}F-DNPs, ^{18}F-DNPs + Tween 80, and ^{18}F-DNPs + PEG$_{8000}$ in contrast with filtered ^{18}F-DNPs, especially at the level of the lung and spleen.

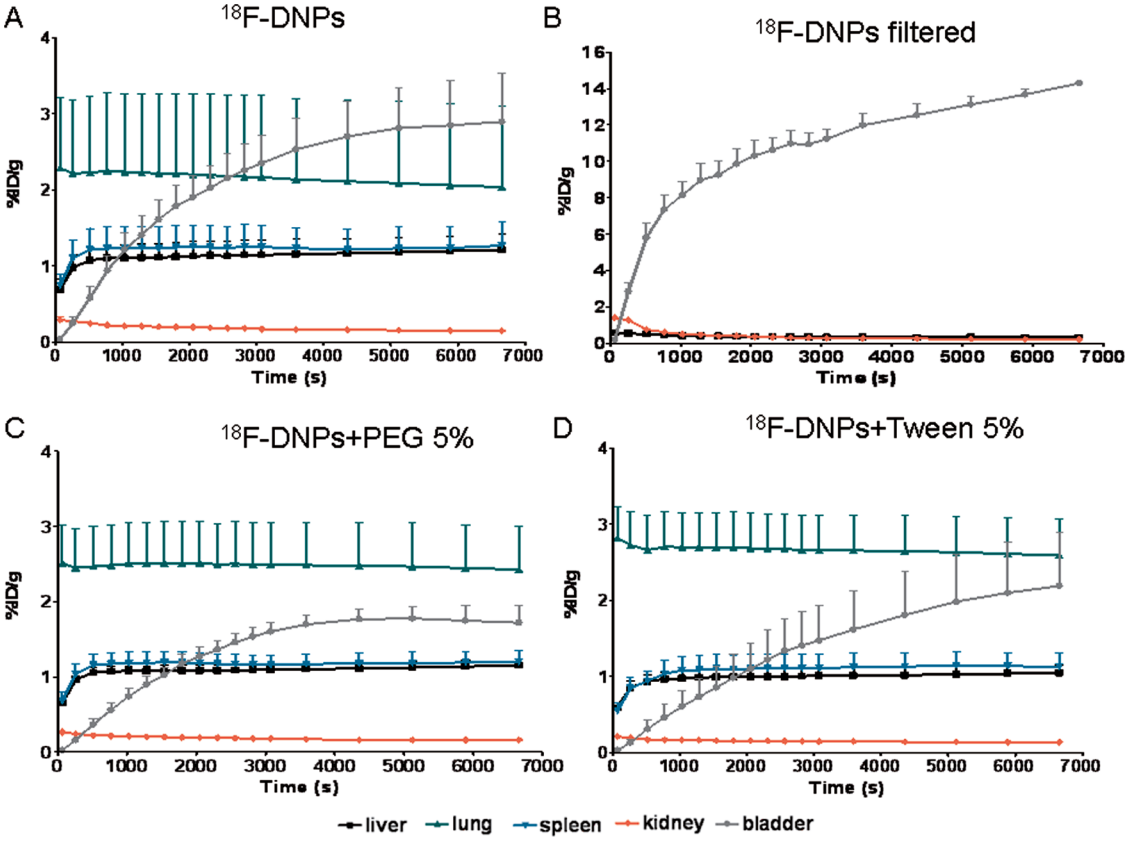

Figure 4. Mean time–activity curves of the different organs obtained from PET images. Bars represent standard deviation. Similar patterns obtained from ^{18}F-DNPs (A), ^{18}F-DNPs + PEG$_{8000}$ (C), and ^{18}F-DNPs + Tween 80 (D). Different patterns were obtained for filtered ^{18}F-DNPs (B). Radioactivity of lungs and spleen was undetectable, and bladder presented higher accumulation of radioactivity.

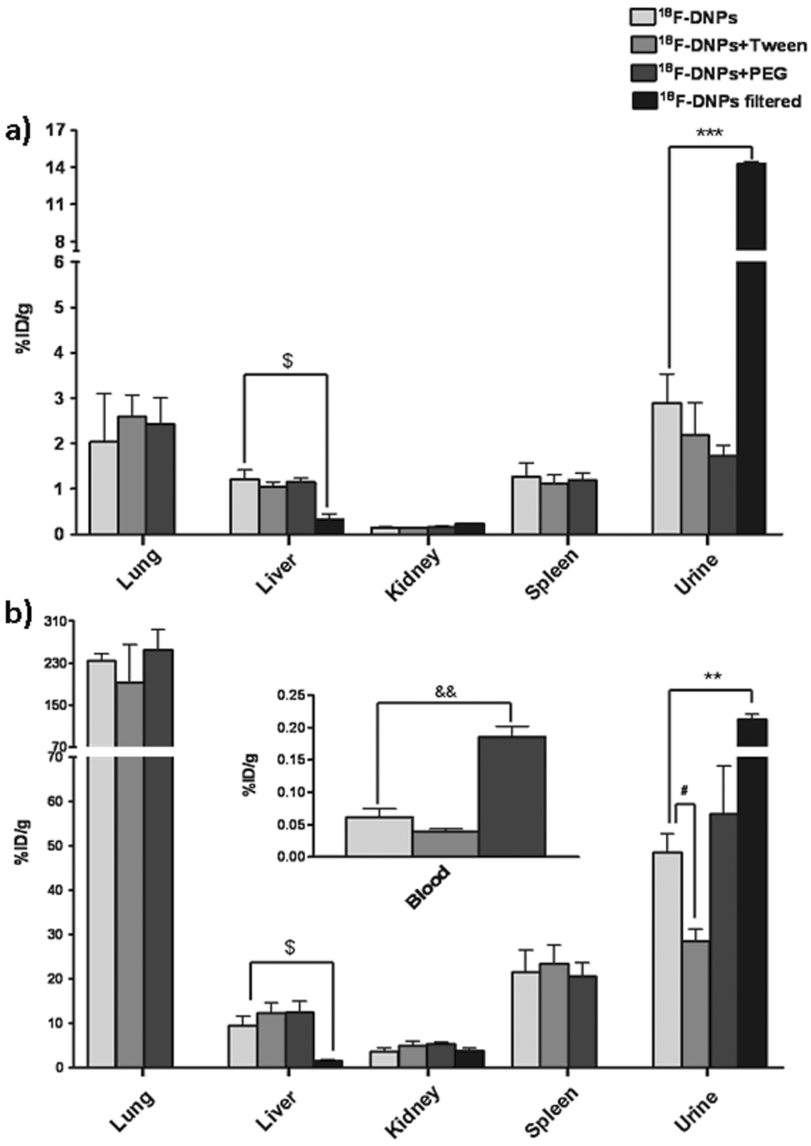

Figure 5. Biodistribution of ^{18}F-DNPs obtained 2 h after administration in (a) rats and (b) mice. Results expressed as percentage of injected dose per gram of tissue (%ID/g) from the PET study showing the biodistribution of ^{18}F-DNPs, filtered ^{18}F-DNPs, and ^{18}F-DNPs supplemented with Tween 80 or PEG_{8000}. Uptake in lung and spleen in filtered ^{18}F-DNPs groups was below the detection limits in both cases. (a) Statistical analysis in rats: Student's *t*-test *($p < 0.001$); $^{\$}$($p = 0.018$). (b) Statistical analysis in mice: Student's *t*-test **($p = 0.002$); $^{\$}$($p = 0.017$); $^{\#}$($p = 0.015$); $^{\&\&}$($p = 0.005$).**

size of the nanoparticle as determined by TEM (about 7 nm in our case) and their kinetic size in aqueous dispersion as determined by laser scattering (around 680 nm).

Influence of Surfactant Agents. In the biodistribution study, visual inspection of the images showed accumulation of the ^{18}F-DNPs mainly in lungs, liver, kidneys, and spleen. The bladder was also clearly visible, especially in the later frames of the dynamic images, which is suggestive of urinary excretion of the radiolabeled compound (Figures 3 and 4). The addition of PEG_{8000} or Tween 80 to the labeled nanoparticles did not significantly modify organ uptake. Radiolabeled nanoparticles with or without surfactants showed the highest concentration in the lungs followed by liver and spleen and finally by the kidneys (Figure 5a). The uptake of ^{18}F-DNPs in the lungs strongly suggests trapping in the capillary pulmonary bed by size exclusion. In contrast, the early rise in uptake observed in the liver and spleen could potentially reflect phagocitosys of ^{18}F-DNPs by the reticuloendothelial system. This system is known to phagocytize foreign materials of sizes similar to the administered nanoparticles and, depending on the particle characteristics, is one of the major causes of nanoparticle removal from blood. The fraction of ^{18}F-DNPs that were not phagocytized was excreted in the urine, as shown by the progressive increase in urine concentration. Usually, the concentration of a compound that is not trapped by phagocytosis decreases in the organs proportionally to the excretion rate. In our case, however, the ^{18}F-DNP concentration in the reticuloendothelial system liver and spleen is kept constant in spite of the observed

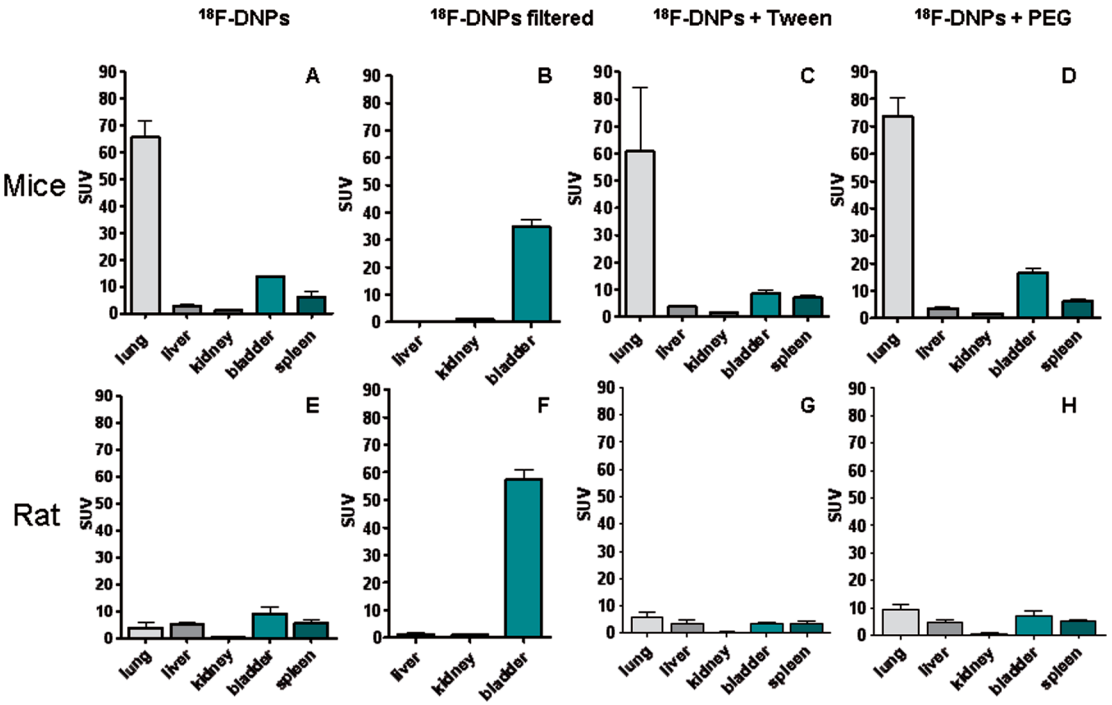

Figure 6. Results from the *ex vivo* study (A–D) and PET (E–H) biodistribution studies expressed as standard uptake values to correct the mass differences between mice and rats. Lungs presented radically different standard uptake value (SUV) in mice than in rats. Uptake in the lung and spleen in filtered ^{18}F-DNPs groups was below the detection limits.

progressive excretion, which is compatible with the trapping of the nanomaterial in macrophages.

The continuous increase in bladder concentration of ^{18}F-DNPs strongly suggests that a fraction of the injected nanoparticles remained in the blood despite the trapping of most of them in the lungs and reticuloendothelial system. Interestingly, ^{18}F-DNPs supplemented with Tween 80 or PEG_{8000} showed a slower urinary excretion rate (Figure 4), suggesting that the addition of these agents could reduce the renal excretion of the nanoparticle and, consequently, increase their bioavailability in the blood, in accordance with previous studies with other nanomaterials.[19−21] Supporting this hypothesis, the bladder activity at the end of image acquisition tended to be lower in animals receiving ^{18}F-DNPs + PEG_{8000} or ^{18}F-DNPs + Tween 80 (Figure 5a).

Similar findings were obtained in the *ex vivo* study in which the addition of PEG_{8000} or Tween 80 only modified the accumulation of ^{18}F-DNPs in blood and urine, respectively (Figure 5b). Animals administrated with ^{18}F-DNPs + Tween 80 showed a significant decrease in urinary concentration of radioactivity (p = 0.015). Analysis of blood samples showed higher levels of radioactivity in animals receiving ^{18}F-DNPs + PEG_{8000} (p = 0.005). These results are in agreement with the PET study in rats, confirming that surfactant agents such as Tween 80 or PEG_{8000} could reduce renal excretion of DNPs and increase their blood bioavailability. Future studies should focus on this effect of stabilizing agents on the blood bioavailability of DNPs.

Influence of Nanoparticle Kinetic Size. In contrast to the lack of influence of surfactant agents, filtration notably changed the biodistribution pattern in the *in vivo* study with rats, especially in the lung and spleen (Figure 4). Time−activity curves reflect these differences between filtered ^{18}F-DNPs and the other three preparations (Figure 4). In the filtered case, the radioactivity content in the lung and spleen was undetectable, and the liver presented a much lower uptake (p = 0.018) than the nonfiltered ^{18}F-DNP groups (Figure 5a). Therefore, ^{18}F-DNPs that passed through the filter were neither trapped in the pulmonary capillary bed by size exclusion nor phagocytized by the reticuloendothelial system. This result confirms that the high uptake in lungs and spleen in the nonfiltered studies was caused by accumulation of the ^{18}F-DNPs with larger kinetic sizes. In contrast, the similar kidney uptake and urinary excretion pattern among all groups is indicative of it being originated by the circulating ^{18}F-DNPs (Figure 4). However, the percentage of injected dose per gram of tissue (%ID/g) in the urine of the filtered ^{18}F-DNPs was 4-fold higher than the other ^{18}F-DNP preparations (p < 0.001) (Figure 5a). An explanation for this fact could be that the lack of trapping in the lungs or reticuloendothelial system would increase the available amount of ^{18}F-DNPs for urinary excretion.

The results obtained in the *ex vivo* study performed in mice were concordant with those obtained by PET in all the tissues, with the exception of the lungs, in which nonfiltered ^{18}F-DNP preparations presented a higher concentration compared to that in rats (Figure 6). To

our knowledge, such behavior has not been previously described for the biodistribution of nanoparticles. This unexpected discrepancy was not caused by the different injected masses between mice and rats, as, after normalization by animal body weight, only in the mice was the ^{18}F-DNPs + PEG_{8000} group higher than that in the rat. One possible explanation for this fact could arise from the different total pulmonary vascular bed size between rats and mice. Purportedly, a smaller pulmonary vascular bed could trap higher amounts of nanocompounds, but further studies are required to pinpoint the exact nature of this phenomenon. This behavior is not normally observed with conventional drugs and, thus, is particularly important for the development of nanocompounds for biomedical applications. With respect to the rest of the organs, the results were in accordance with those found with PET. Filtration completely eliminated the uptake in the lungs and spleen and significantly reduced it in the liver ($p = 0.005$). On the other hand, the concentration of radioactivity in the urine at the end of the study was significantly higher in comparison to nonfiltered ^{18}F-DNPs ($p = 0.002$).

In summary, DNPs were properly labeled with ^{18}F by reacting ^{18}F-SFB on ω-aminopropyl-functionalized, Fenton-treated DNPs. In the rodent biodistribution study, ^{18}F-DNPs were mainly retained in the lungs and reticuloendothelial system probably by size exclusion and phagocytosis, respectively. ^{18}F-DNPs with a kinetic particle size small enough not to be trapped in the pulmonary capillary bed or the reticuloendothelial system were finally excreted in the urine. Apparently, the addition of suspension surfactant agents such as Tween 80 and PEG_{8000} had little effect on the biodistribution of ^{18}F-DNPs but could reduce their urinary excretion, thereby increasing the blood bioavailability. Although our biodistribution study refers to a specific DNP derivative with amino functional groups, it is reasonable to assume that most of the conclusions are valid for many other functionalized DNPs with similar hydrophilicity and kinetic sizes. In this regard, our study shows that quantitative biodistribution studies are extremely useful and informative for future evaluations of nanoparticles as therapeutic agents.

MATERIALS AND METHODS

Study Design and Statistical Analysis. The biodistribution of the ^{18}F-labeled DNPs was evaluated under four different formulations: (i) suspended in saline; (ii) suspended in saline and filtered trough a 0.45 μm hydrophilic filter, (iii) suspended in saline containing 5% Tween 80; and (iv) suspended in saline with 5% PEG_{8000}. The effect of filtration and addition of surfactants was evaluated both *in vivo* in rats and *ex vivo* in mice. Between-group concentrations of ^{18}F-labeled DNPs in the different organs were compared by Student's *t*-tests, setting a threshold for statistical significance of $p < 0.05$.

Materials and Instrumentation. All the reactants for synthesis including the DNPs were purchased from Advanced Biochemical Compounds (Radeberg, Germany), Sigma-Aldrich (Madrid, Spain), and Scharlab (Sentmenat, Spain). QMA, C18 HELA cartridges were obtained from Waters (Cerdanyola del Vallès, Spain), and animals from Charles River (France). The cyclotron used for ^{18}F production was an 18/9 model from IBA (Louvain-la-Neuve, Belgium). Analytical and purification HPLC were obtained with an Agilent 1100 series coupled to a diode array UV−vis Agilent 100 detector (Madrid, Spain) and a Raytest GINA isotopic detector (Barcelona, Spain). The centrifuge used was a Hettich-Zentrifugen (Tuttlingen, Germany).

HO-DNP Production. Commercial DNPs (1 g) were suspended in distilled water (50 mL) in a 500 mL open flask and mixed directly with $FeSO_4 \cdot 7H_2O$ (5 to 20 g) as a source of Fe^{2+}. After complete dissolution of the ferrous salt, concentrated sulfuric acid (30 mL) was added to the slurry, and the corresponding volume of H_2O_2 (30 v/v%) (20 mL) was slowly dropped while observing evolution of CO_2. Caution has to be taken, as H_2O_2 is a strong oxidant and the Fenton reaction at high concentration is highly exothermic, occurring with evolution of heat and gases. Thus, the process has to be done in a well-ventilated fume hood wearing the appropriate personal safety items. This slurry was sonicated on an ice-refrigerated ultrasound bath and held at 1−5 °C for 5 h.

After the Fenton treatment, the suspensions were diluted with distilled water and allowed to reach room temperature. The excess of acid was removed by five consecutive centrifugation−redispersion cycles with Milli-Q water. HO-DNPs sediment occurred at the bottom of the centrifuge tube under these conditions. The pH value of the supernatant at the fifth centrifugation−redispersion cycle was neutral. Finally, the Fenton-treated DNPs were submitted to overnight freeze-drying to obtain a brownish dust-like material. The increase in the population of OH groups was determined by monitoring the intensity of the OH stretching band in quantitative IR spectroscopy.

3-Aminopropyltriethoxysilane (50 mg) was suspended in dry acetonitrile (15 mL); then Fenton-treated DNPs (200 mg) were added. The mixture was stirred for 20 h at reflux temperature and then cooled at room temperature and filtered. The solid was washed with methanol and dichloromethane. The amino-functionalized DNP was dialyzed for 3 days using a membrane in distilled water in order to remove the excess of the silyl reagent.

The degree of functionalization was determined by different techniques (see Supporting Information). Finally, the size of the nanoparticle was determined by TEM, and the kinetic size in aqueous dispersion was determined by laser scattering and atomic force microscopy (AFM). TEM experiments were carried out using a Philips CM300 FEG system at an operating voltage of 100 kV. As for the AFM measurements, 2 μL of colloidal NH2-npD solution was deposited on a fresh piece of graphite (1 × 1 cm) and allowed to adsorb for 2 min at room temperature. Imaging was performed under dry conditions in air with 250 μm long cantilevers with a resonance frequency of about 8 kHz. No image processing was carried out in the presented image. Size measurements were performed using a Zetasizer Nano ZS (Malvern Instruments, UK) to determine the size of the colloidal aqueous solutions of NH_2-npD. A 5 mg amount of NH_2-npD was suspended in 100 mL for measurements, which were carried out in an automatic mode. The size values were averaged after 30 runs (Figure 1).

***N*-Succinimidyl 4-[^{18}F]Fluorobenzoate (^{18}F-SFB).** The synthesis was done in assembled Eckert & Ziegler modules following the methodology described in ref 15. Briefly, $^{18}F^-$ was produced in the cyclotron by bombardment of [^{18}O]-H_2O with high-energy protons (18 MeV). The $^{18}F^-$ was sent to the automatic module, where it was trapped in a QMA cartridge. Then, it was extracted toward the reactor by transferring a mixture of 2 mg

of K_2CO_3 and 1.8 mg of Kryptofix 222 in 1 mL of a mixture of H_2O/CH_3CN (1:1) through the QMA cartridge. The reactor was heated at 100 °C, and in order to dry the $^{18}F^-$ present, He flow and vacuum were applied for 5 min. To ensure that the drying process was done successfully, an extra 1 mL of anhydrous CH_3CN was added, drying the mixture as before. The next step consisted in adding a solution of 5 mg of 4-(*tert*-butoxycarbonylmethyl)phenyl trimethylammonium trifluoromethanesulfonate in 1 mL of anhydrous CH_3CN. The mixture was stirred for 10 min at 90 °C, and then, 0.5 mL of 1 M HCl was added. The reaction mixture was heated at 100 °C for 5 min. After cooling to 25 °C, the reaction mixture was diluted with 9 mL of water and passed through a C18 HELA cartridge for solid extraction. Subsequently, 3 mL of CH_3CN was passed through the cartridge and the solution was sent to a second reactor. This eluate was treated with 20 μL of 25% methanolic Me_4NOH in 500 μL of CH_3CN. Then, the reaction mixture was dried at 90 °C, passing a continuous He flow and applying vacuum. Drying was completed by the addition of 3 mL of anhydrous CH_3CN. After, a solution of 15 mg of *N,N,N′,N′*-tetramethyl-*O*-(*N*-succinimidyl-)uronium tetrafluoroborate in 500 μL of anhydrous CH_3CN was added, and the mixture was heated at 90 °C for 2 min. The mixture was cooled to 25 °C and diluted with 5% aqueous acetic acid. The reaction crude was purified by semipreparative HPLC using a Teknokroma Mediterranean Sea-18 (25 × 1 cm, 5 μm) column and working in isocratic mode with a mobile phase composed by CH_3CN/ammonium formate (3.15 g/1 L H_2O, pH = 5) (42.5:57.5) at a flow rate of 5 mL/min and monitored by gamma and UV−vis (254 nm) detectors. The desired fraction (9−11 min) was collected over 20 mL of a 0.9% saline solution. This solution was passed through a C18 cartridge, rinsed with 20 mL of water, and extracted with 3 mL of anhydrous acetone. The solvent was dried by bubbling N_2, the residue was solved in 200 μL of DMSO, and an aliquot was submitted to quality testing. Quality control was done by HPLC using a Teknokroma Mediterranean Sea-18 (25 × 0.46 cm, 5 μm) column and working at 2 mL/min in gradient mode using CH_3CN/ammonium formate (3.15 g/1 L H_2O, pH = 5) as mobile phase starting with a mixture 10:90 and achieving 40:60 in 10 min. The detection was monitored by gamma and UV−vis (254 nm) detectors, obtaining ^{18}F-SFB at 10.3 min. With this methodology, ^{18}F-SFB was obtained with a yield of 37 ± 5%, with chemical and radiochemical purity exceeding 98% and 102 ± 7 GBq/μmol of specific activity.

^{18}F-labeled DNP Production. A 2.0 ± 0.3 mg amount of ω-aminopropyl-functionalized DNPs was stirred at room temperature for 1.5 h with a solution composed of aproximately 70 mCi of pure ^{18}F-SFB in a mixture of 150 μL of DMSO and 100 μL of phosphate buffer at pH = 7.4. After this, 1.8 mL of phosphate buffer at pH = 7.4 was added, and the mixture was centrifuged at 4000 rpm for 10 min. The resultant solid was washed twice by centrifugation at 4000 rpm using 2 mL of phosphate buffer. After checking the absence of radioactivity in the liquid of the centrifuged dispersion, the washed ^{18}F-DNP solid was dispersed in 2 mL of the desired solvent (physiologic saline/physiologic saline + 5% Tween 80/physiologic saline + 5% PEG_{8000}) and sonicated for 5 min just before injection. In one preparation the dispersion was passed through a 0.45 μm hydrophilic filter. Using the described procedure a radiochemical yield of 21.3 ± 4% was obtained after washing. A scheme summarizing the nanodiamond production is shown in Figure 2.

Animals. For the *in vivo* PET biodistribution study, adult male Sprague−Dawley rats weighing 375 ± 49 g (mean ± standard deviation; Charles River, France; *n* = 14) were used. The *ex vivo* study was performed in male and female adult Swiss CD1 mice weighing 29 ± 1 g (mean ± standard deviation; Charles River, France; male *n* = 6, female *n* = 6). Animals were housed in controlled laboratory conditions with the temperature maintained at 21 ± 1 °C and humidity at 55 ± 10%. Food and water were available *ad libitum*. Animal procedures were conducted in strict accordance with the guidelines of the European Communities Directive 86/609/EEC regulating animal research and were approved by the local ethical committee (CEEA-PRBB).

PET Image Acquisition. Animals were anesthetized with isoflurane and received an intravenous bolus injection of the ^{18}F-radiolabeled nanoparticle preparation. Doses administered were 5.7 ± 0.9 MBq for the ^{18}F-DNP dispersed in saline (*n* = 4); 1.5 ± 0.9 MBq for the filtered DNPs (*n* = 3); 23.4 ± 11.9 MBq for ^{18}F-DNP in saline with 5% Tween 80 (*n* = 4); and 22.4 ± 3.3 MBq for ^{18}F-DNP with 5% PEG_{8000} (*n* = 3). Immediately after injection, the animals were placed in an animal-dedicated camera (microPET R4; Concorde, Siemens, Knoxville, TN, USA) for dynamic whole body image acquisition. Whole body data were acquired for 120 min. During all the acquisition procedure anesthesia was maintained with a facial mask and a concentration of 2.5% isoflurane vaporized in O_2.

Image Analysis. To obtain the dynamic whole body images (frames = 18), PET data were corrected for nonuniformity, random coincidences, and radionuclide decay and reconstructed with a filtered backprojection algorithm into a matrix size of 128 × 128, a voxel size of 0.85 × 0.85 mm, a slice thickness of 1.21 mm, and an axial field of view covering the full length of the animal (approximately 20 cm). After reconstruction, volumes of interest were manually drawn for the different organs, and the individual time−activity curves were obtained. Activity concentration at the end of the acquisition was used to calculate the percentage of injected dose per gram of tissue and the standard uptake value. Mean time−activity curves of the four animal groups were also derived for each organ.

***Ex Vivo* Study.** For the *ex vivo* biodistribution study, animals were anesthetized with isoflurane, given an intravenous bolus injection of the ^{18}F-labeled nanoparticle preparation, and returned to their cages. The injected doses were 1.6 ± 0.1 MBq for the DNPs dispersed in saline (*n* = 3); 0.12 ± 0.01 MBq for filtered DNPs (*n* = 3); 1.6 ± 0.9 MBq for DNPs in 5% Tween 80 (*n* = 3); and 7.1 ± 0.6 MBq for DNPs in 5% PEG_{8000} (*n* = 3). After 120 min, animals were sacrificed, and the different organs were dissected, weighed, and measured in a gamma counter (Wallac 1470 Wizard, Perkin-Elmer, Waltham, MA, USA) for ^{18}F radioactivity determination. The experimental radioactivity data were corrected for decay, injected dose, mass of the tissue sample, and animal weight to obtain the percentage of injected dose per gram of tissue and the standard uptake values, respectively.

Acknowledgment. The present work was supported by Spanish MICINN (Grant CTQ-2009-11586); the Fondo de Investigación Sanitaria (FIS) of the Instituto de Salud Carlos III (Grants PS09/02620, PI10/1195, and PS09/02217), La Marató TV3 Foundation (Grant 090530), and CDTI under the CENIT Programme (AMIT Project) and supported by the Spanish Ministry of Science and Innovation. R.M. thanks the Spanish Ministry for a postgraduate scholarship. V.M.V. is a recipient of Fondo de Investigacion Sanitaria (FIS) and Generalitat Valenciana contract (CES10/030)

Supporting Information Available: Full characterization (IR, laser scattering, *z*-potential, ^{19}F NMR, TEM, and AFM) of the different nanodiamonds obtained or used in the present study and a preparation method to obtain the ^{19}F-DNPs are available free of charge via the Internet at http://pubs.acs.org.

REFERENCES AND NOTES

1. Kim, B. Y.; Rutka, J. T.; Chan, W. C. Nanomedicine. *N. Engl. J. Med.* **2010**, *363*, 2434–2443.
2. Liang, X. J.; Chen, C.; Zhao, Y.; Jia, L.; Wang, P. C. Biopharmaceutics and Therapeutic Potential of Engineered Nanomaterials. *Curr. Drug Metab.* **2008**, *9*, 697–709.
3. Yang, H. Nanoparticle-Mediated Brain-Specific Drug Delivery, Imaging, and Diagnosis. *Pharm. Res.* **2010**, *27*, 1759–1771.
4. Milane, L.; Duan, Z. F.; Amiji, M. Pharmacokinetics and Biodistribution of Ionidamine/Paclitaxel Loaded, EGFR-Targeted Nanoparticles in an Orthotopic Animal Model of Multi-Drug Resistant Breast Cancer. *Nanomedicine* **2010**, *in press*.
5. Martin, R.; Alvaro, M.; Herance, J. R.; Garcia, H. Fenton-Treated Functionalized Diamond Nanoparticles as Gene Delivery System. *ACS Nano* **2010**, *4*, 65–74.
6. Prencipe, G; Tabakman, S. M.; Welsher, K.; Liu, Z.; Goodwin, A. P.; Zhang, L.; Henry, J.; Dai, H. PEG Branched Polymer for

Functionalization of Nanomaterials with Ultralong Blood Circulation. *J. Am. Chem. Soc.* **2009**, *131*, 4783–4787.
7. Balasubramanian, S. K.; Jittiwat, J.; Manikandan, J.; Ong, C. N.; Yu, L. E.; Ong, W. Y. Biodistribution of Gold Nanoparticles and Gene Expression Changes in the Liver and Spleen after Intravenous Administration in Rats. *Biomaterials* **2010**, *31*, 2034–2042.
8. Texier, I.; Josser, V. In Vivo Imaging of Quantum Dots. *Methods Mol. Biol.* **2009**, *544*, 393–406.
9. Shokeen, M.; Fettig, N. M.; Rossin, R. Synthesis, In Vitro and In Vivo Evaluation of Radiolabeled Nanoparticles. *Q. J. Nucl. Med. Mol. Imaging* **2008**, *52*, 267–277.
10. Ambruosi, A.; Yamamoto, H.; Kreuter, J. Body Distribution of Polysorbate-80 and Doxorubicin-Loaded [^{14}C]Poly(butyl cyanoacrylate) Nanoparticles after i.v. Administration in Rats. *J. Drug Target.* **2005**, *13*, 535–542.
11. Chrastina, A.; Schnitzer, J. E. Iodine-125 Radiolabeling of Silver Nanoparticles for In Vivo SPECT Imaging. *Int. J. Nanomed.* **2010**, *5*, 653–659.
12. Rossin, R.; Muro, S.; Welch, M. J.; Muzykantov, V. R.; Schuster, D. P. In Vivo Imaging of ^{64}Cu-Labeled Polymer Nanoparticles Targeted to the Lung Endothelium. *J. Nucl. Med.* **2008**, *49*, 103–111.
13. Martín, R.; Menchón, C.; Apostolova, N.; Victor, V. M.; Alvaro, M.; Herance, J. R.; García, H. Nano-Jewels in Biology. Gold and Platinum on Diamond Nanoparticles as Antioxidant Systems Against Cellular Oxidative Stress. *ACS Nano* **2010**, *4*, 6957–6965.
14. Krueger, A. Diamond Nanoparticles: Jewels for Chemistry and Physics. *Adv. Mater.* **2008**, *20*, 2445–2449.
15. Mading, P.; Fuchtner, F.; Wust, F. Module-Assisted Synthesis of the Bifunctional Labelling Agent N-Succinimidyl 4-[(18)F]Fluorobenzoate ([(18)F]SFB). *Appl. Radiat. Isot.* **2005**, *63*, 329–332.
16. Lam, R.; Ho, D. Nanodiamonds as Vehicles for Systemic and Localized Drug Delivery. *Expert. Opin. Drug Delivery* **2009**, *6*, 883–895.
17. Martin, R.; Heydorn, P. C.; Alvaro, M.; Garcia, H. General Strategy for High-Density Covalent Functionalization of Diamond Nanoparticles Using Fenton Chemistry. *Chem. Mater.* **2009**, *21*, 4505–4514.
18. Zhu, Z. Detonation of Molecular Precursors as a Tool for the Assembly of Nano-Sized Materials. *Mod. Phys. Lett. B* **2003**, *17*, 1477–1493.
19. He, X.; Nie, H.; Wang, K.; Tan, W.; Wu, X.; Zhang, P. In Vivo Study of Biodistribution and Urinary Excretion of Surface-Modified Silica Nanoparticles. *Anal. Chem.* **2008**, *80*, 9597–9603.
20. Liu, Z.; Davis, C.; Cai, W.; He, L.; Chen, X.; Dai, H. Circulation and Long-Term Fate of Functionalized, Biocompatible Single-Walled Carbon Nanotubes in Mice Probed by Raman Spectroscopy. *Proc. Natl. Acad. Sci. U. S. A.* **2008**, *105*, 1410–1415.
21. Schipper, M. L.; Iyer, G.; Koh, A. L.; Cheng, Z.; Ebenstein, Y.; Aharoni, A.; Keren, S.; Bentolila, L. A.; Li, J.; Rao, J.; *et al.* Particle Size, Surface Coating, and PEGylation Influence the Biodistribution of Quantum Dots in Living Mice. *Small* **2009**, *5*, 126–134.